Electronic Supplementary Material (ESI) for Journal of Materials Chemistry A.
This journal is © The Royal Society of Chemistry 2018

Electronic Supplementary Information

Phase-controllable synthesis of MOF-templated maghemite-carbonaceous composites for efficient photocatalytic hydrogen production

Juan Yao, Junying Chen*, Kui Shen, and Yingwei Li*

State Key Laboratory of Pulp and Paper Engineering, School of Chemistry and Chemical Engineering, South China University of Technology, Guangzhou 510640, China.

*To whom correspondence should be addressed

E-mail: chenjunying2010@sina.com, liyw@scut.edu.cn

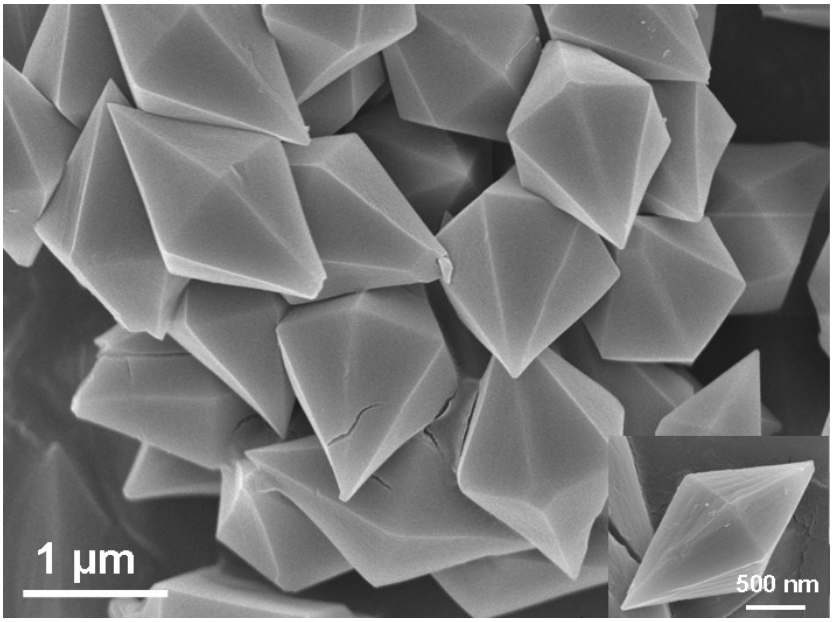

Fig. S1 SEM image of MIL-88B (B-0). The inset shows a single spindle-like particle of MIL-88B (B-0).

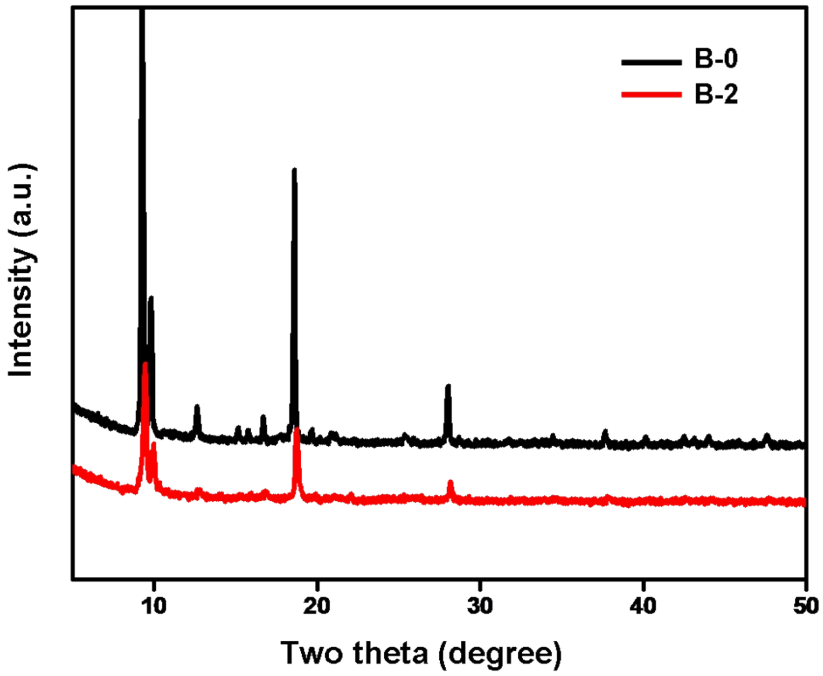

Fig. S2 Powder XRD patterns of B-0 and B-2.

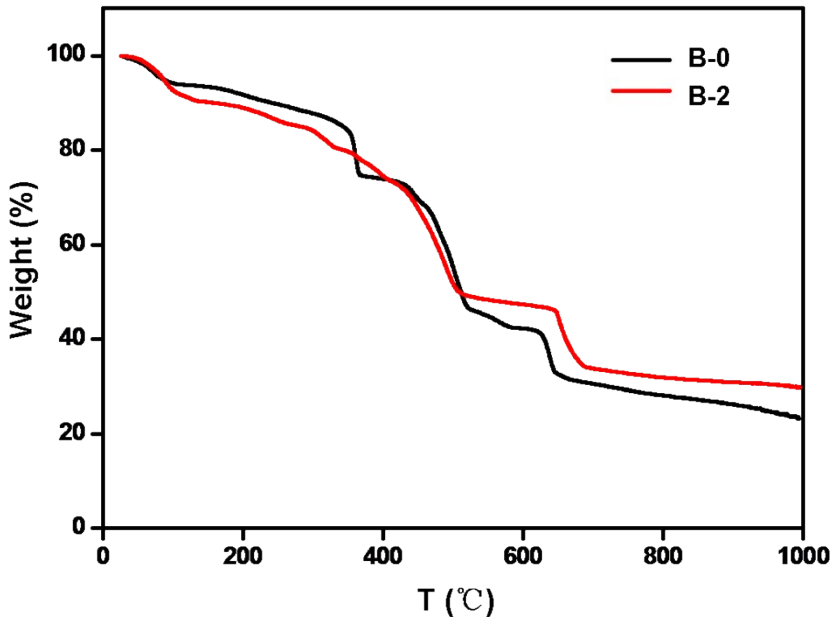

Fig. S3 TGA curves of B-0 and B-2.

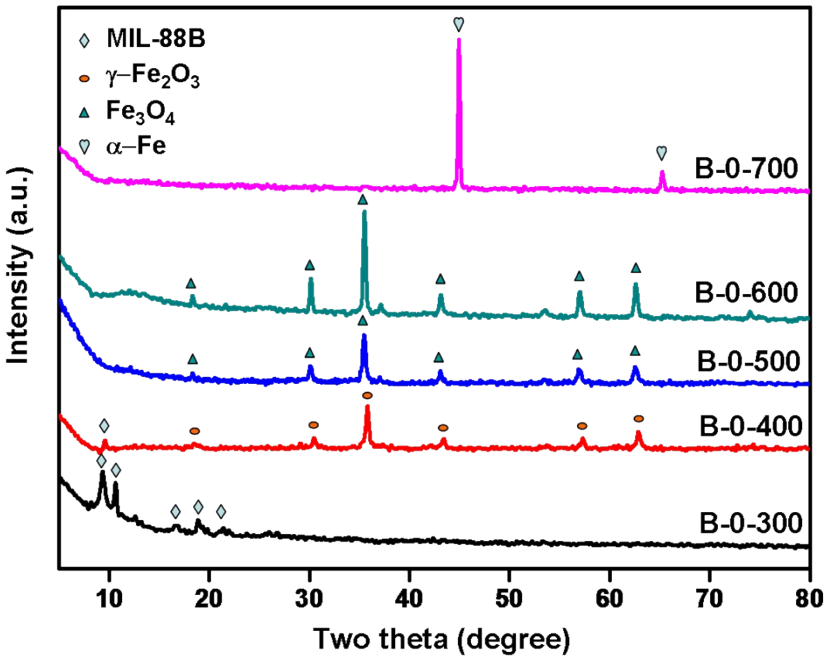

Fig. S4 Powder XRD patterns of samples obtained by thermolysis of B-0 at different temperatures under N_2 atmosphere.

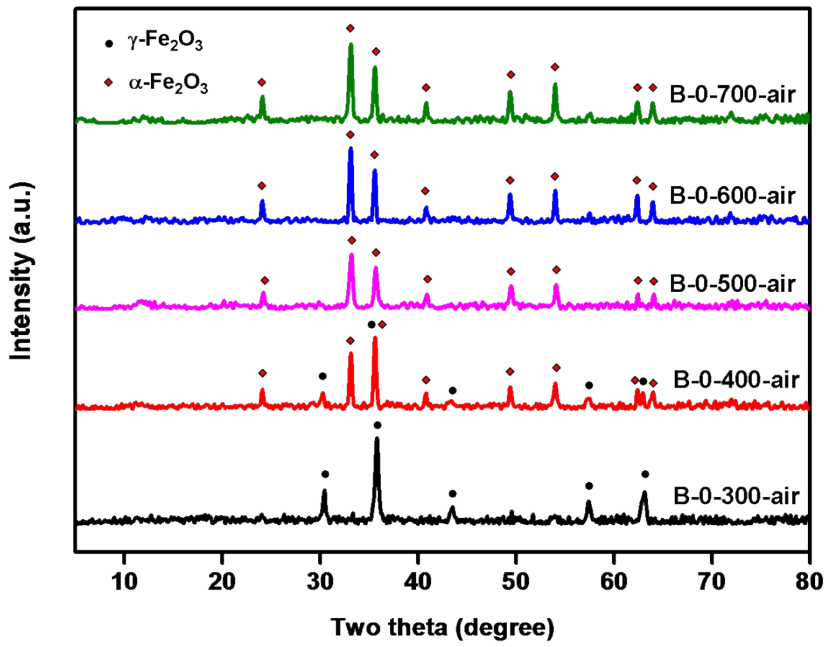

Fig. S5 Powder XRD patterns of samples obtained by thermolysis of B-0 at different temperatures under air atmosphere.

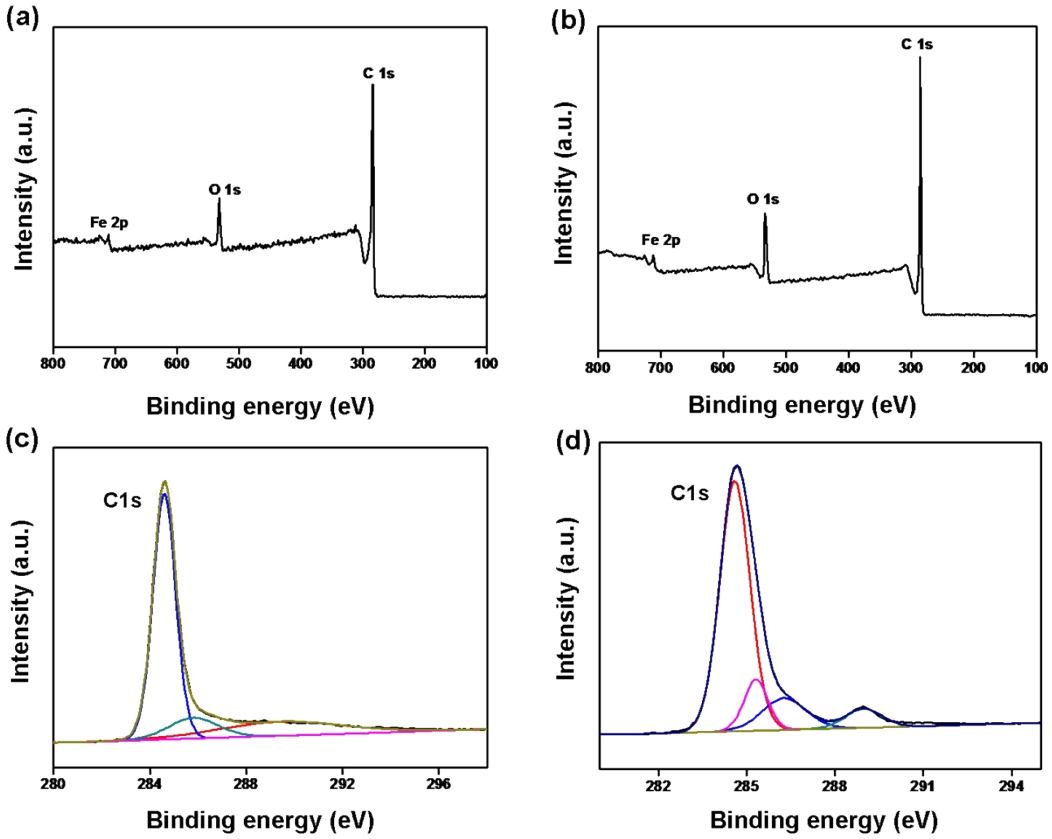

Fig. S6 XPS spectra of B-0-600 (a) and B-2-600 (b); (c) and (d) are the high-resolution XPS spectra of C 1s for B-0-600 and B-2-600, respectively.

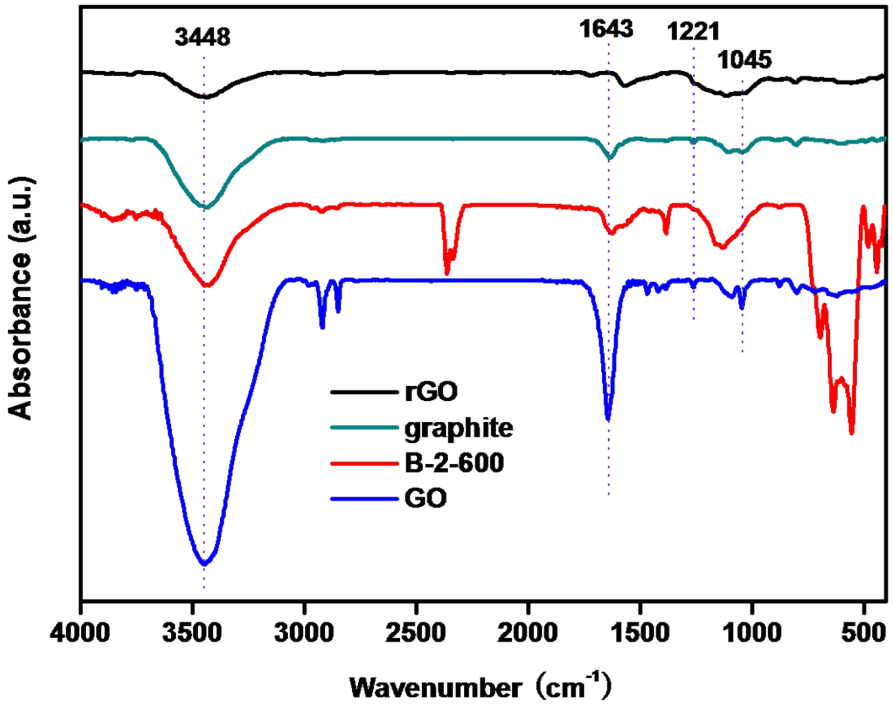

Fig. S7 FT-IR spectra of rGO (black), commercial graphite powder (green), B-2-600 (red) and GO (blue). The position and intensity of the peak around 2365 and 2337 cm^{-1} in the spectrum of B-2-600 should be ascribed to the presence of atmospheric CO_2.

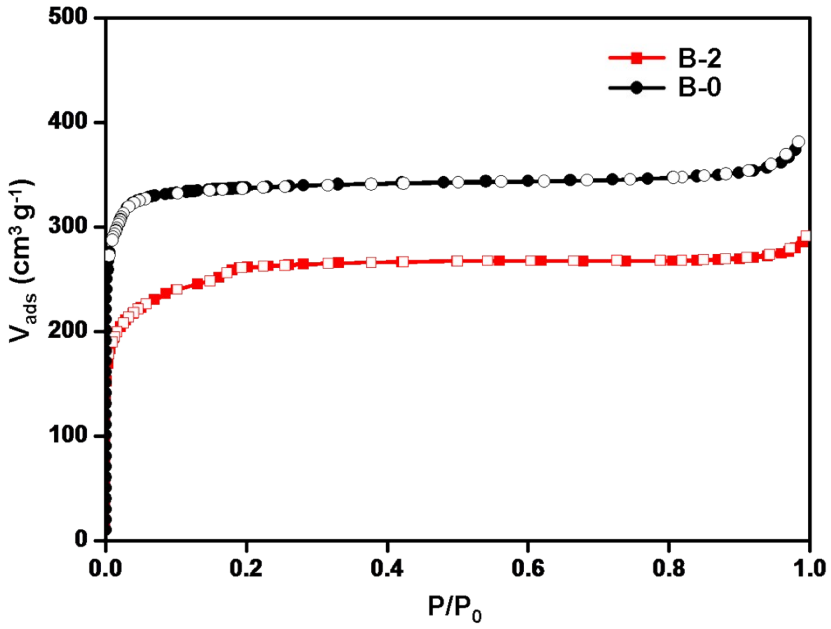

Fig. S8 Nitrogen absorption/desorption isotherms at 77 K of the as-synthesized B-0 and B-2.

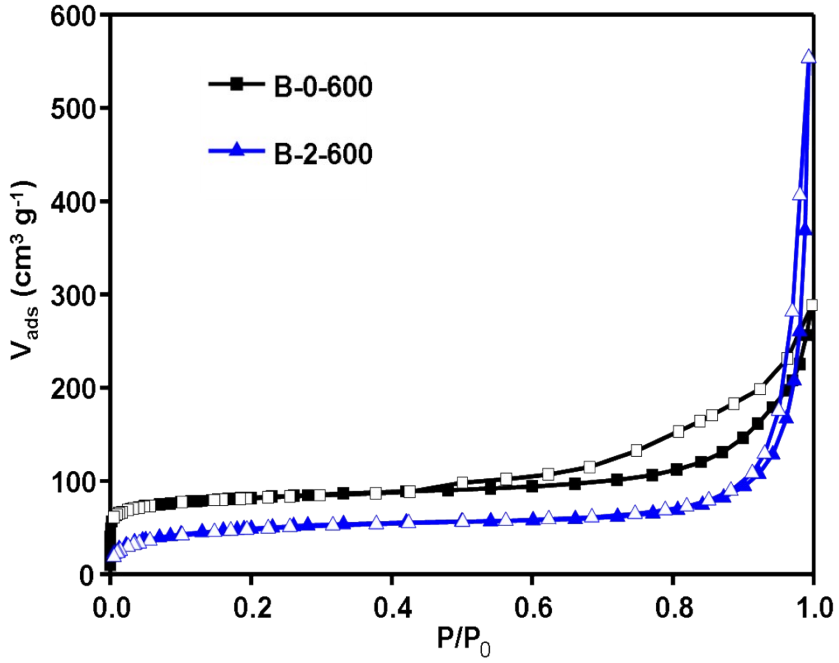

Fig. S9 Nitrogen absorption/desorption isotherms at 77 K of B-0-600 and B-2-600.

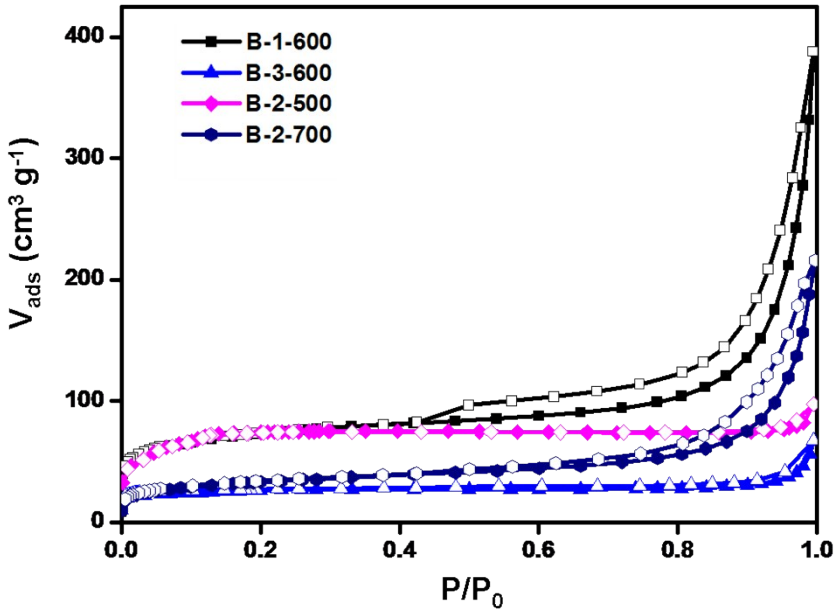

Fig. S10 Nitrogen absorption/desorption isotherms at 77 K of B-1-600, B-2-500, B-2-700 and B-3-600.

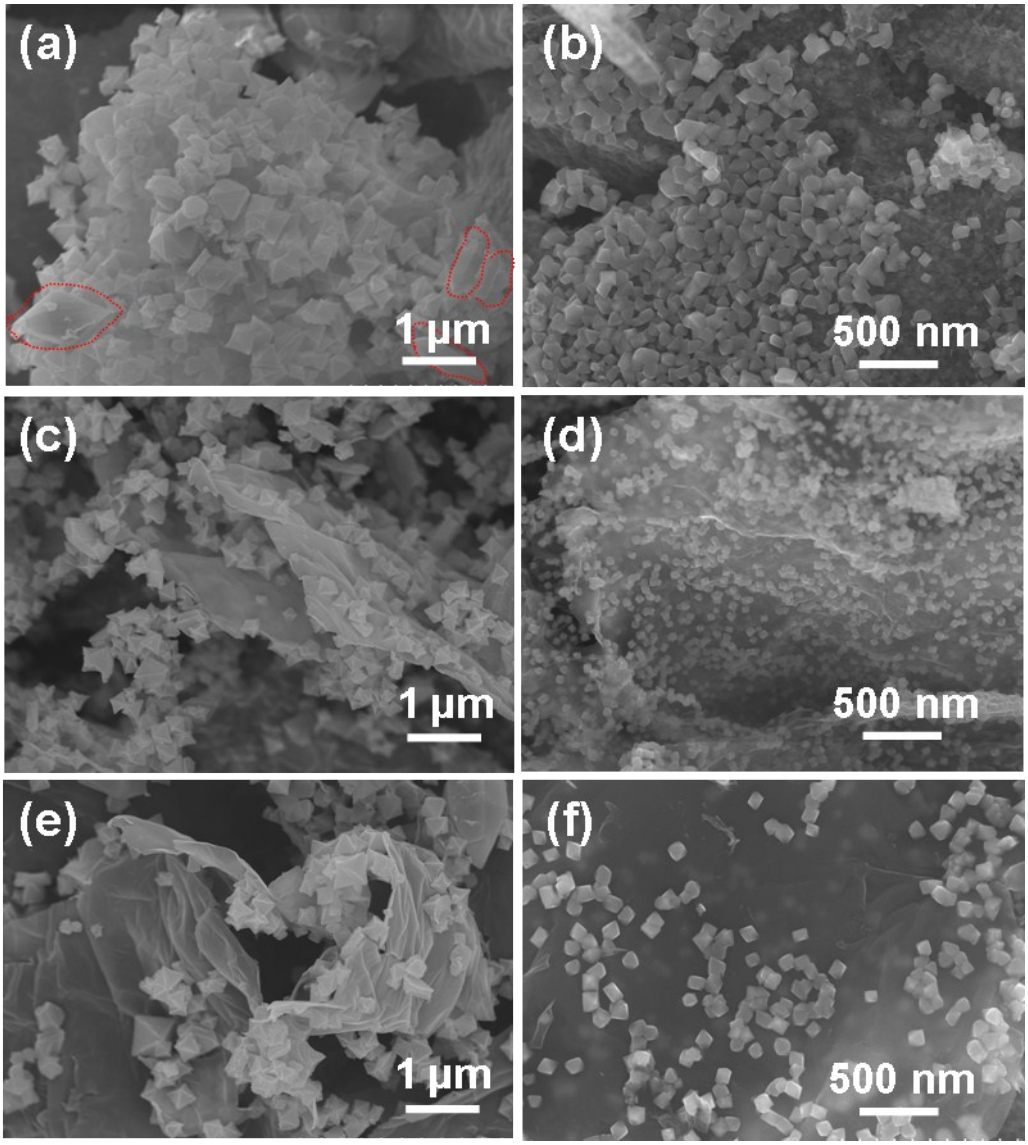

Fig. S11 SEM images of (a) B-1, (b) B-1-600, (c) B-2, (d) B-2-600, (e) B-3 and (f) B-3-600.

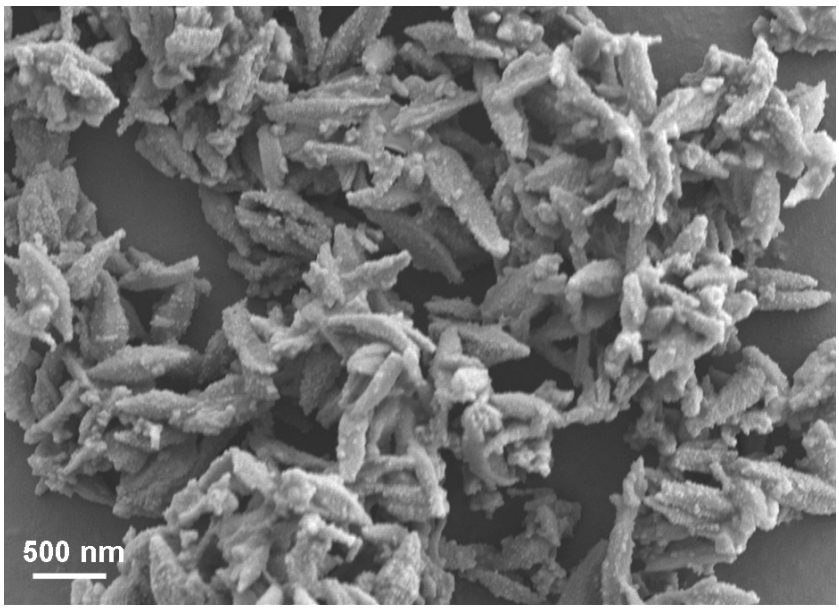

Fig. S12 SEM image of B-0-600.

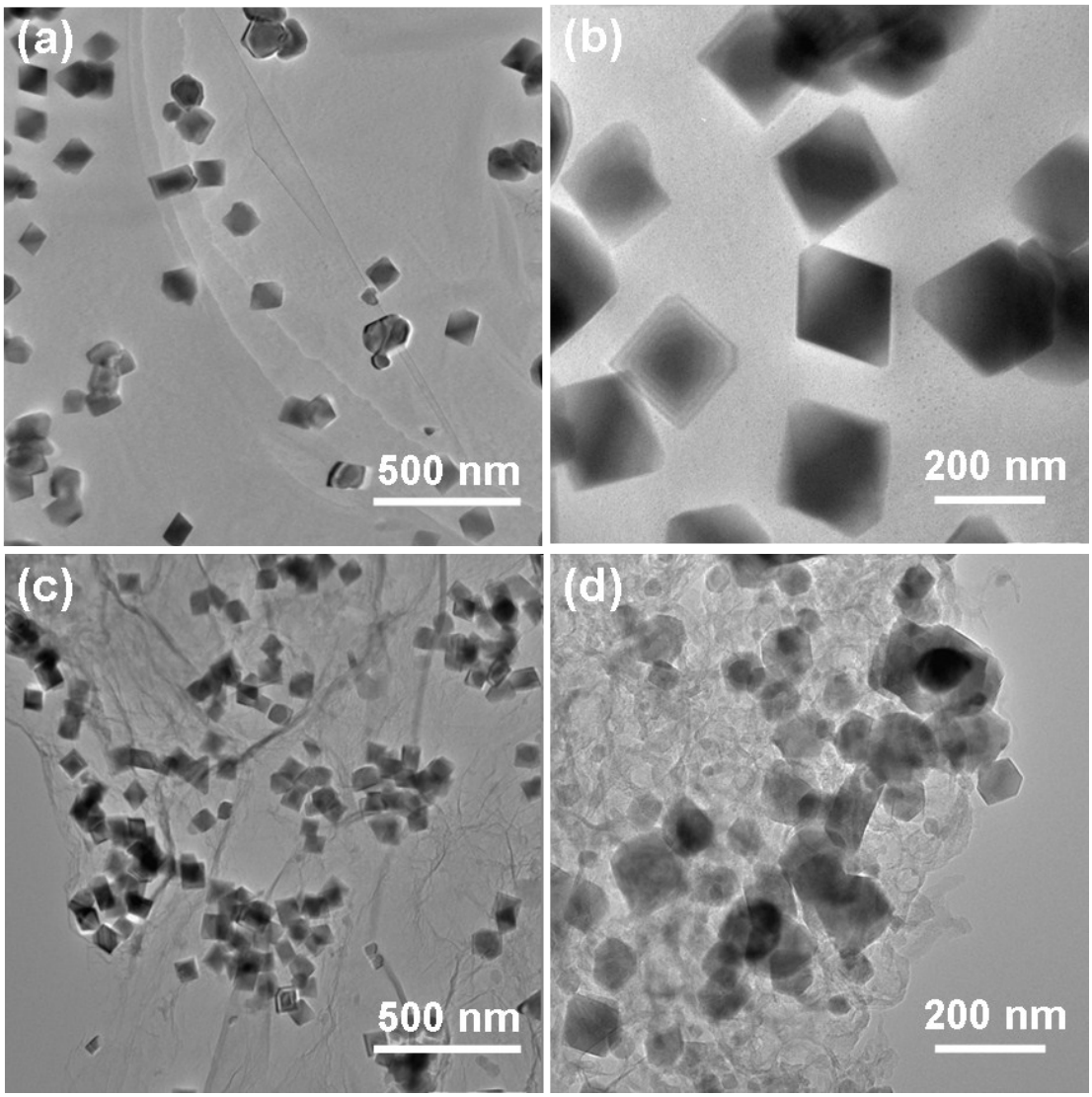

Fig. S13 TEM images of (a, b) B-1-600 and (c, d) B-3-600.

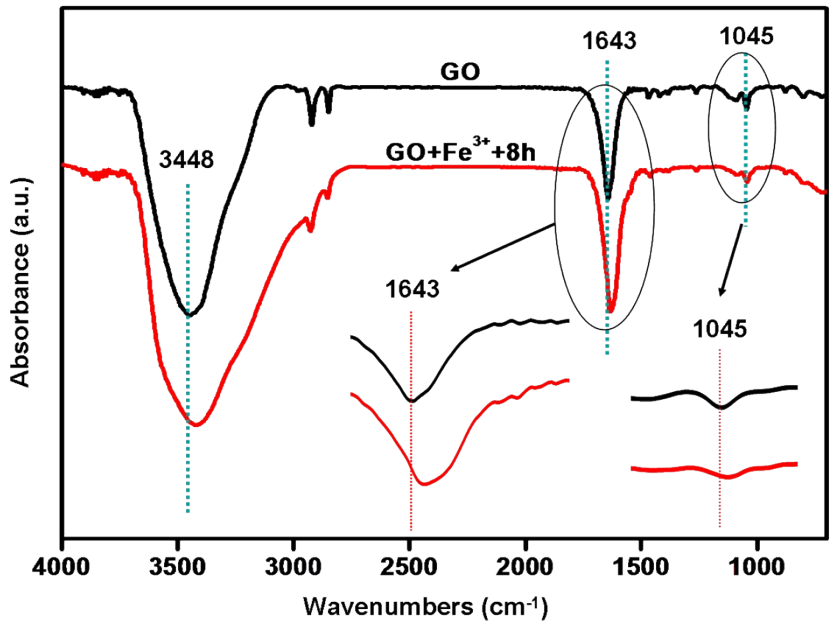

Fig. S14 FT-IR spectra of GO (black) and the mixture of GO and Fe^{3+} (red) after treatment under ultrasonication for 8 h.

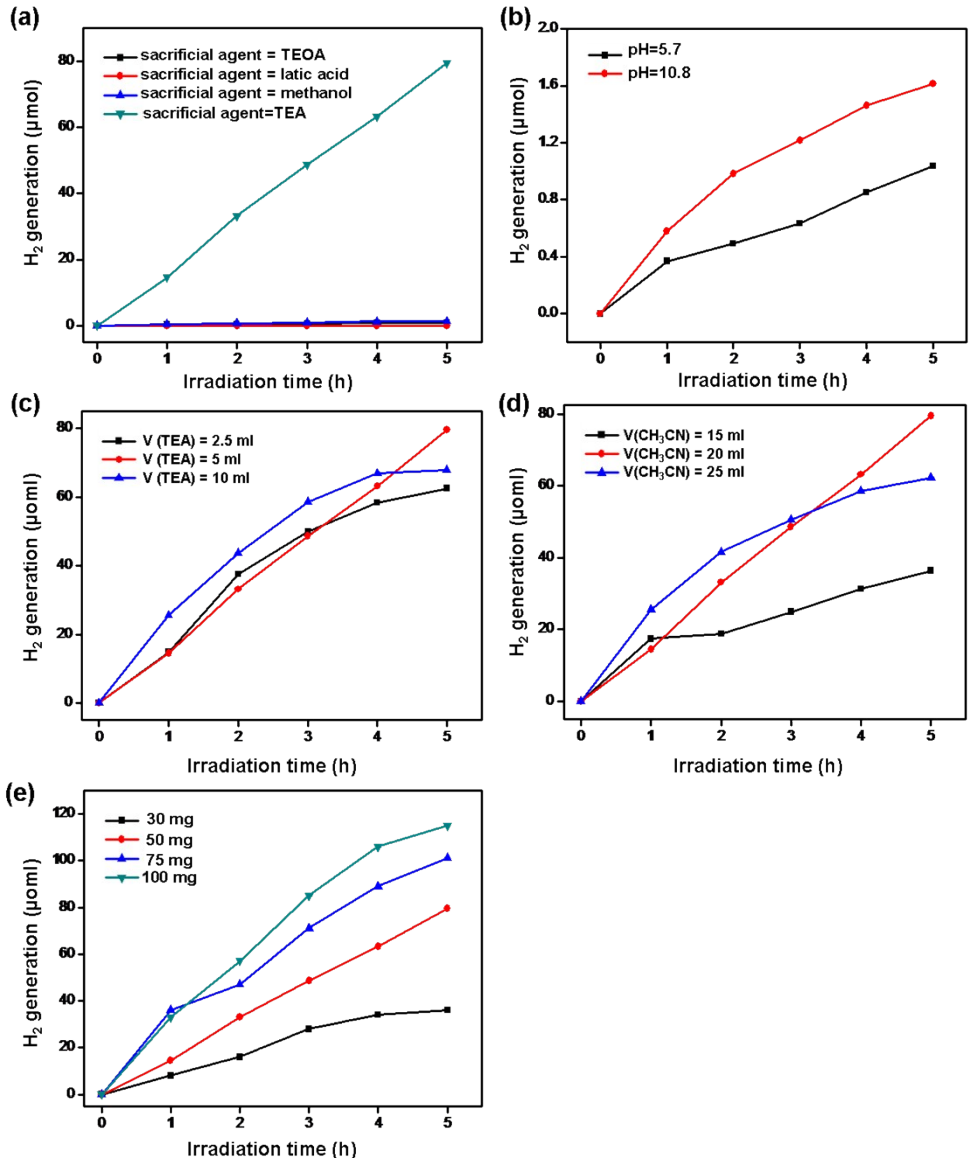

Fig. S15 Time courses of photocatalytic H_2 production under conditions of varied sacrificial agents (a) and pH values (b), varied volume ratio of H_2O: CH_3CN: TEA (c and d) and amounts of B-2-600 (e).

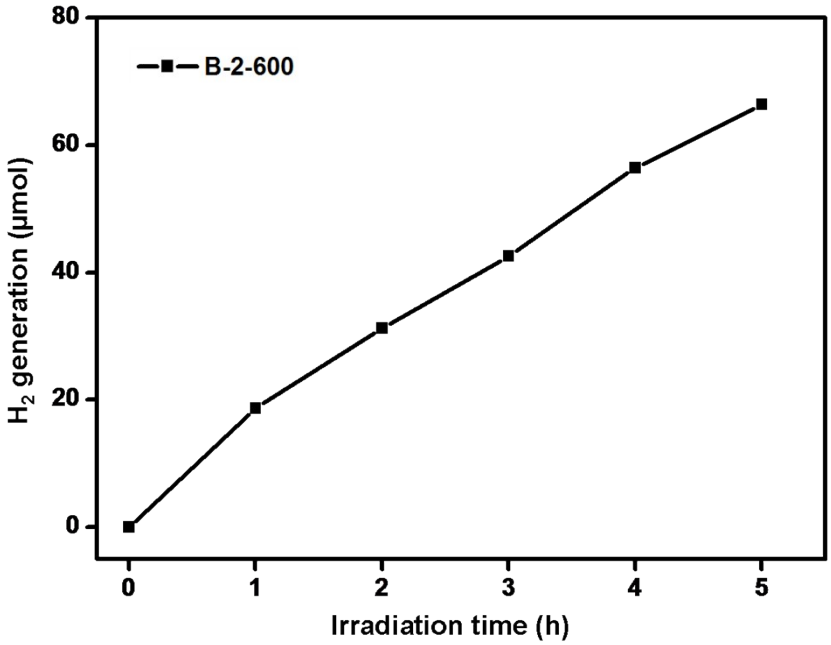

Fig. S16 Time course of photocatalytic H_2 production by B-2-600 under visible-light irradiation by Xe lamp with a 400 nm cut-off filter.

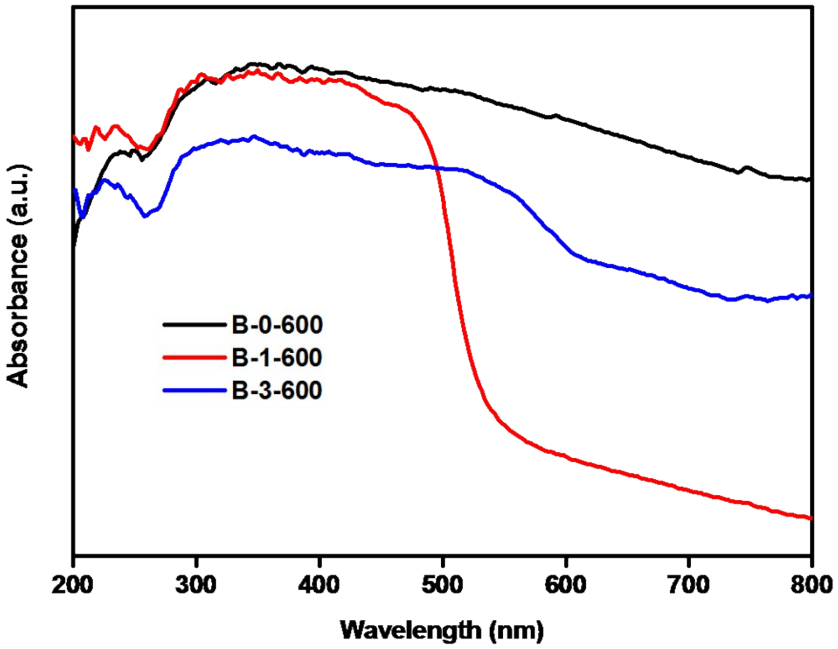

Fig. S17 UV-vis DRS spectra of B-0-600, B-1-600 and B-3-600.

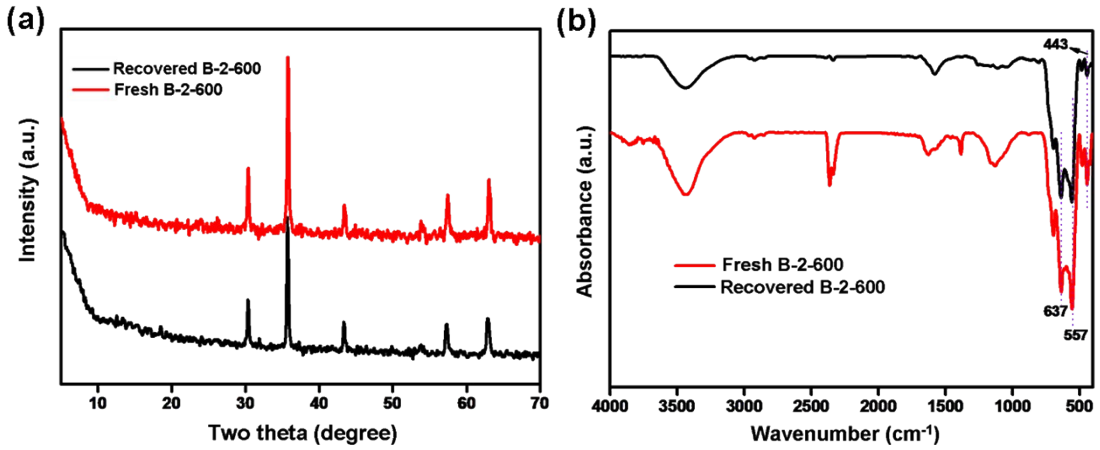

Fig. S18 (a) Powder XRD patterns and (b) FTIR spectra of as-prepared B-2-600 and B-2-600 after 4 cycles.

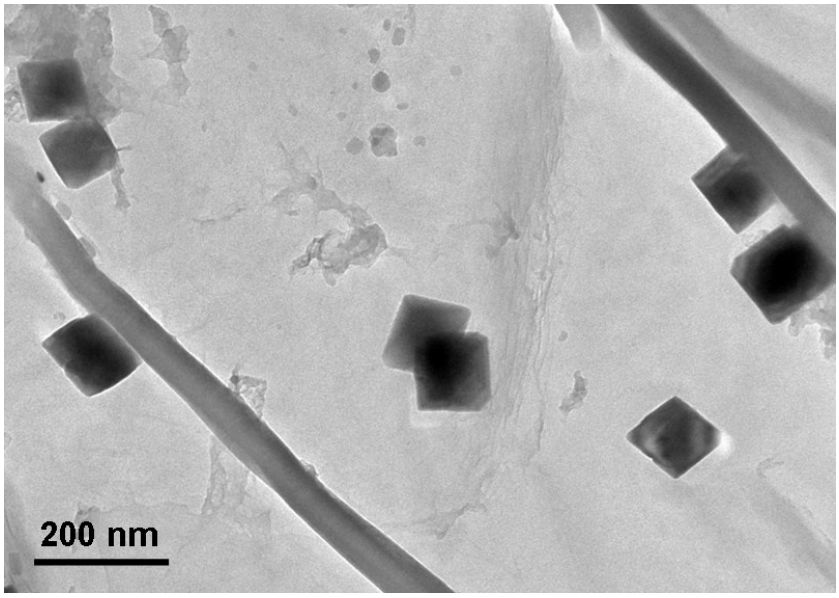

Fig. S19 TEM image of B-2-600 after 4 cycles.

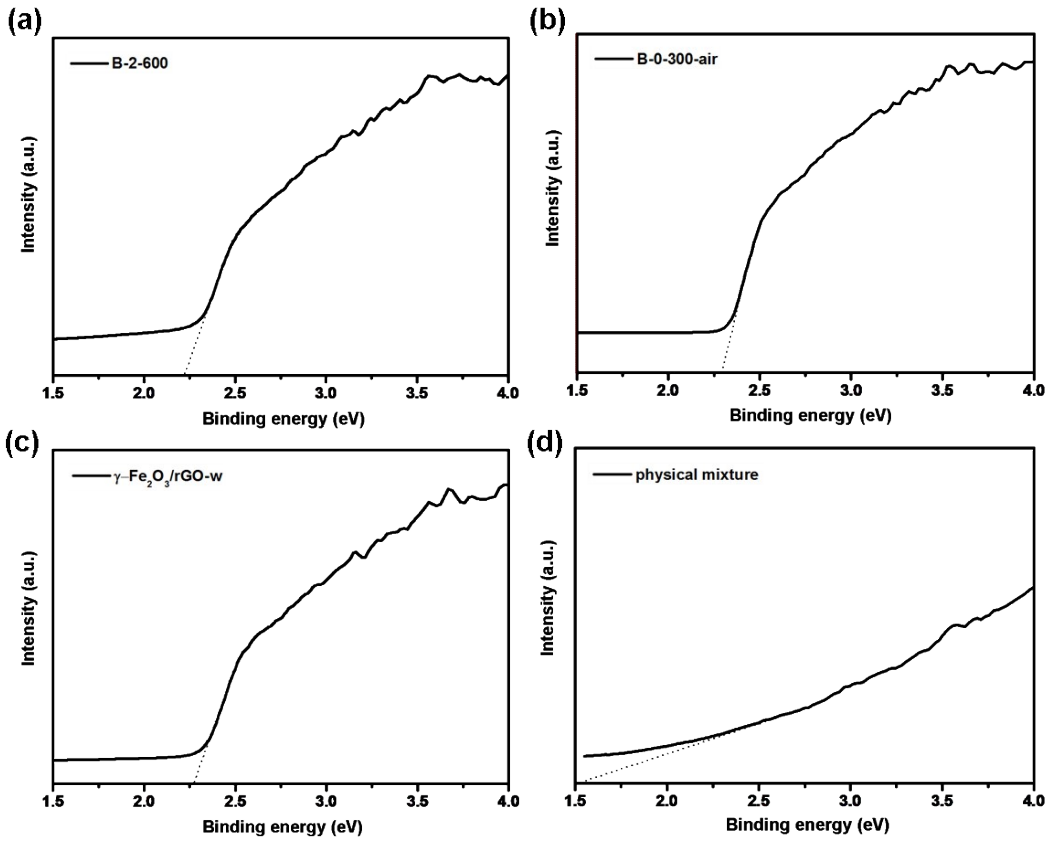

Fig. S20 Estimated band gap energy of (a) B-2-600, (b) B-0-300-air and (c) γ-Fe_2O_3/rGO-w using Kubelka-Munk equation: $(\alpha h\upsilon)^2 = A(E_g - h\upsilon)$, where h is Planck'sconstant, υ is the frequency of light, and A is a constant. E_g of each material was deduced by plotting $(\alpha h\upsilon)^2$ *vs.* hυ and extrapolating the straight part to x-axis. The intersect was read as the E_g for the certain material.

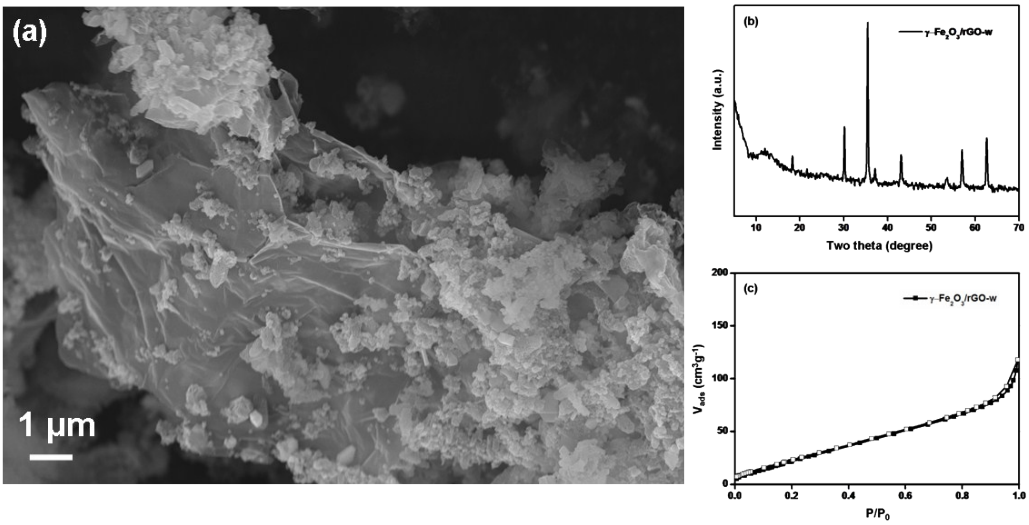

Fig. S21 (a) SEM image, (b) powder XRD patterns and (c) nitrogen absorption/desorption isotherms at 77 K of γ-Fe_2O_3/rGO-w.

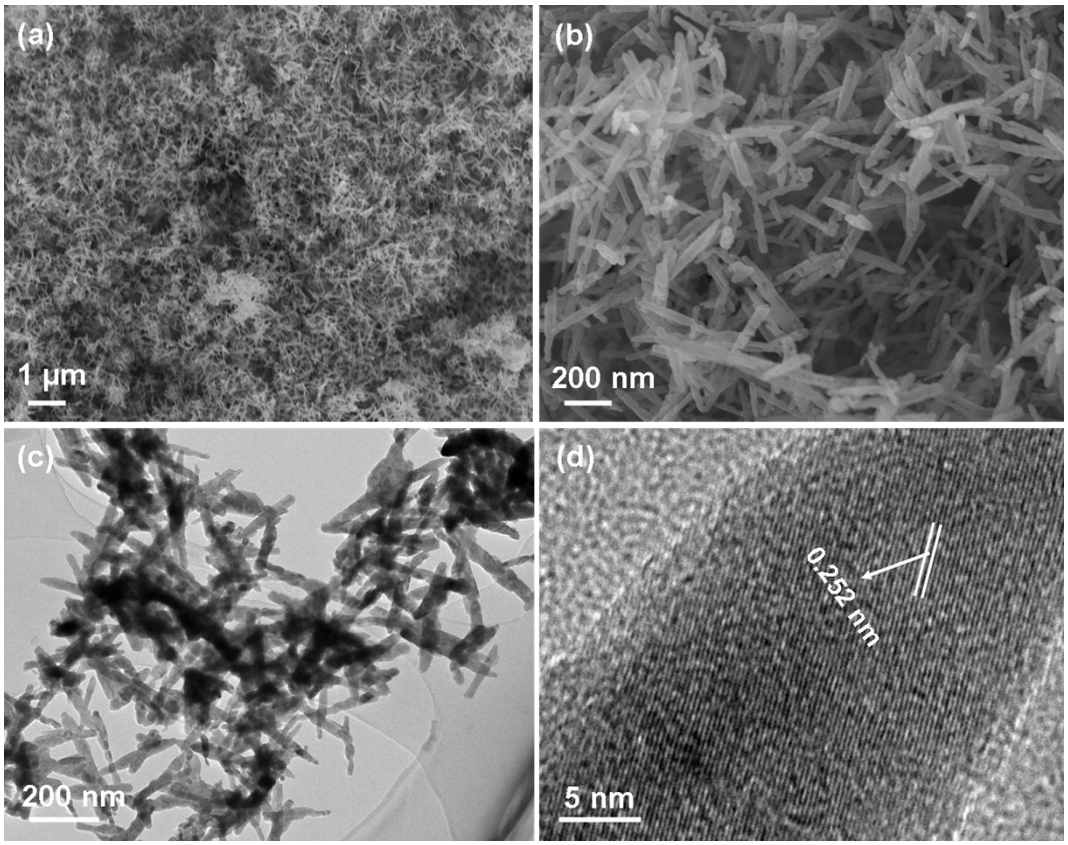

Fig. S22 (a, b) SEM, (c) TEM and (d) HRTEM image of B-0-300-air. The lattice spacing of 0.252 nm was assigned to the {311} plane of γ-Fe_2O_3.

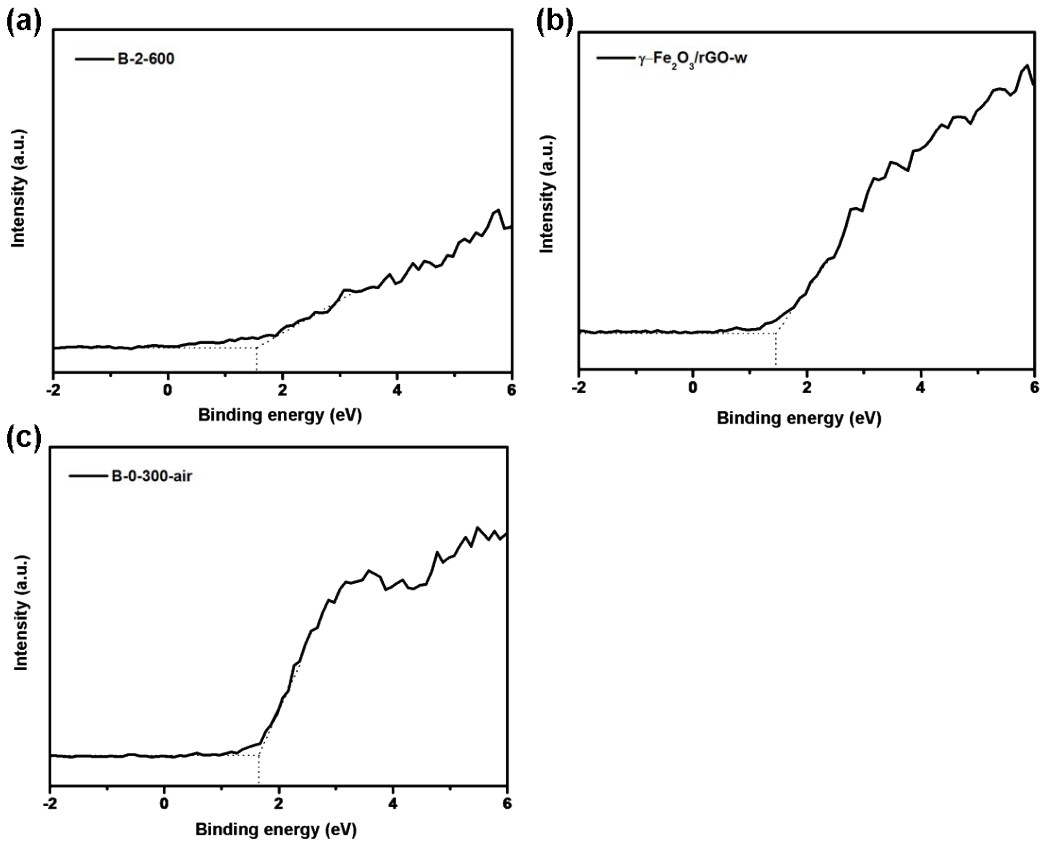

Fig. S23 Valence-band (VB) XPS spectra of (a) B-2-600, (b) γ-Fe_2O_3/rGO-w and (c) B-0-300-air.

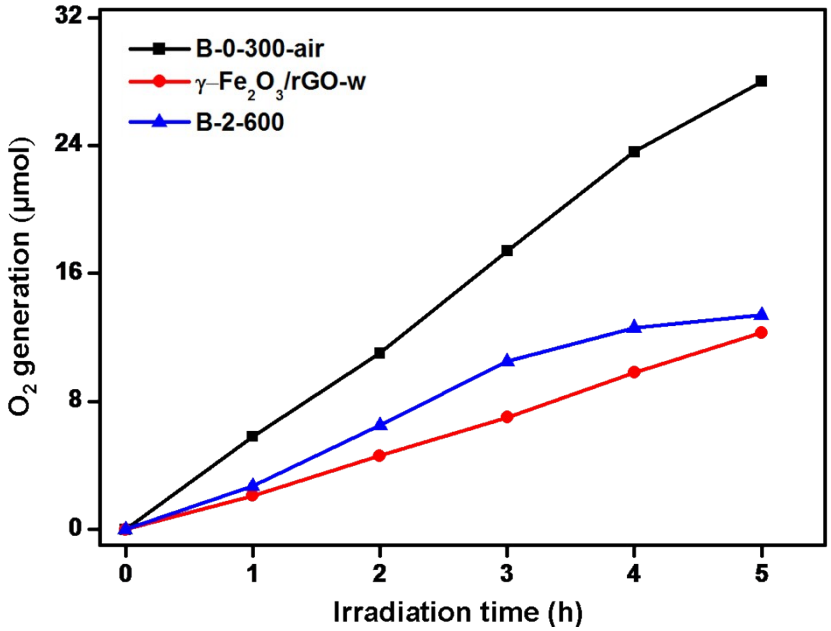

Fig. S24 Time course of photocatalytic O_2 evolution in the presence of $AgNO_3$ by B-0-300-air, B-2-600 and γ-Fe_2O_3/rGO-w.

Table S1 Characterization results of the catalysts

Sample	S_{BET} (m^2g^{-1})	Pore volume (cm^3g^{-1})	Content (wt%)			
			C[a]	H[a]	O[b]	Fe[c]
MIL-88B	1173.7	0.43	37.5	3.6	33.2	24.3
B-2	940.1	0.41	39.2	4.1	31.8	23.6
B-0-600	282.3	0.13	53.2	0.4	13.1	32.4
B-1-600	258.3	0.12	54.3	0.7	17.2	26.2
B-2-600	173.4	0.08	55.2	0.6	20.0	23.1
B-3-600	87.0	0.15	56.0	0.2	18.0	24.0
B-2-500	243.1	0.10	54.8	1.5	19.5	23.3
B-2-700	115.3	0.18	33.2	0.3	13.0	49.5
γ-Fe_2O_3/rGO-w	92.3	0.04	54.9	2.3	15.7	24.6
B-0-300-air	29.8	0.014	5.8	0.6	32.0	60.6

[a] Measured by elemental analysis. [b] Calculated. [c] Measured by AAS.

Table S2 Optimization of reaction parameters for photocatalytic H_2 production

Entry	Catalysts amount (mg)	V_{H2O} (ml)	$V_{solvent}$[a] (ml)	V_{Sa} (ml)	SA	pH	Rate (μmol g^{-1} h^{-1})
1	50	45.0	0	5	TEOA	11.2	3.7
2	50	45.0	0	5	lactic acid	6.7	0.0
3	50	45.0	0	5	Methanol	7.3	5.4
4	50	27.5	20	2.5	TEA	10.6	250.0
5[b]	50	25.0	20	5	TEA	10.8	6.4
6[c]	50	25.0	20	5	TEA	5.7	4.1
7	50	25.0	20	5	TEA	10.8	318.0
8	50	20.0	20	10	TEA	12.0	272.0
9	50	30.0	15	5	TEA	11.6	142.7
10	50	20.0	25	5	TEA	11.1	249.2
11	30	25.0	20	5	TEA	10.8	240.0
12	75	25.0	20	5	TEA	10.8	269.3
13	100	25.0	20	5	TEA	10.8	230.0

[a] Solvent is CH_3CN. [b, c] phosphate buffer solutions were used to adjust the pH values of solutions. SA is Sacrificial agent.

Table S3 Recyclability of B-2-600 in photocatalytic H_2 production

Cycle	Catalyst Amount (mg)[a]	H_2 evolved in 5 h (μmol)	Rate (μmol g^{-1} h^{-1})
1st	50.0	79.5	318.0
2nd	47.5	76.1	320.4
3rd	45	73.3	325.6
4th	42.5	69.1	325.2

[a]The weight of the catalyst before and after one cycle of photocatalysis reaction is measured in the presence of a stirring bar. A portion (average of 2.5 mg for triple tests) of catalyst lost during recovery procedures.